Accepted Manuscript

The influence of the healing agent characteristics on the healing performance of epoxy coatings: assessment of the repair process by EIS technique

Mohammad Sadegh Koochaki [1,2], Rasoul Esmaeely Neisiany [3], Saied Nouri Khorasani [1,*], Ali Ashrafi [4],

Stefano P. Trasatti [2] and Mirko Magni [2]

[1]   Department of Chemical Engineering, Isfahan University of Technology, Isfahan, 84156-83111,

       Iran

[2]   Department of Environmental Science and Policy, Università degli Studi di Milano, Milan

       20133, Italy

[3]   Department of Materials and Polymer Engineering, Hakim Sabzevari University, Sabzevar,

       9617976487, Iran

[4]   Department of Material Engineering, Isfahan University of Technology, Isfahan, 84156-83111,

       Iran

*   Corresponding author's email: saied@iut.ac.ir

Abstract

The effects of the healing agents' molecular characteristics were studied on the self-healing

performance of the epoxy coatings via corrosion evaluation techniques. Methylene diphenyl

diisocyanate (kept constant) and different polyetheramine healing agents were encapsulated

separately in poly(styrene-co-acrylonitrile) through the electrospray method and added to

the epoxy matrix to prepare a polyurea-based dual capsule extrinsic healing system.

Commercial grades of polyetheramine, Jeffamine D230, Jeffamine D400, and Jeffamine

T403, were used to study the effects of molecular weight and functionality. Scanning

electron microscopy (SEM) and transmission electron microscopy (TEM) images revealed

the formation of spherical shape with multicore morphology for the prepared

polyetheramine containing microcapsules (MCs). Successful encapsulation was evaluated

27   by Fourier transform infrared spectroscopy (FTIR), while the encapsulation yield was

28   measured by thermogravimetric analysis (TGA). Electrochemical Impedance Spectroscopy

29   (EIS) was employed to monitor the corrosion behavior of a series of coated carbon steel

30   samples through the evolution of the impedance spectra, and the numerical values of the

31   related electrical equivalent circuit components (*e.g.*, corrosion resistance), of the scratched

32   coatings at different exposure times in a near-neutral 3.5 wt.% NaCl solution. The results

33   revealed the adverse effect on the corrosion protection ability by increasing the healing

34   agent's molecular weight, while an increase of its functionality improved the final healing

35   efficiency of the coating. According to the EIS results, the maximum healing efficiency was

36   determined to be 85%, 72%, and 90% for Jeffamine D230, Jeffamine D400, and Jeffamine

37   T403, respectively.

39

1. Introduction

Polymeric materials are of broad interest as thin films when acting as a protecting layer to hamper the corrosion process, an exergonic reaction, that can detrimentally affect the mechanical properties of metallic materials resulting in failures [1, 2]. However, polymers are prone to failure caused by external factors that decrease the efficacy of using them in practical applications [3-5]. Among all the proposed solutions for this problem, the concept of self-healing polymeric materials has gained considerable attention [6-9]. The key mechanism in the self-healing process is stopping the crack growth (induced from an external factor) by reducing the crack-tip stress intensity by producing a wedge of polymerized healing agent. These mechanisms require the healing agent to be sufficiently polymerized after release [10-12]. Different strategies have been used to assure the recovery in the self-healing polymers according to their applications and use [13-16]. The ability to retard and ultimately arrest fatigue cracks hinges on the ability of the healing chemistry to produce the polymer in the crack plane at a rate that is comparable to the rate of crack propagation [17]. Therefore, several types of research have been conducted to study the effects of healing agents' characteristics on healing kinetics and efficiency [18].

Jones and coworkers reported different healing performances for the several crystal morphologies of Grubbs' catalyst. They found that smaller catalyst particles can dissolve easier in dicyclopentadiene (DCPD) monomers and perform faster healing reactions. However, they are more susceptible to deactivation by the amine molecules present in the matrix. Their conclusions imply the necessity of having a balance between different crystal morphologies/dimensions to assure the best healing performance [19]. In another research, they investigated the effects of catalyst recrystallization and wax protection to take the advantage of faster healing kinetics without being suffered by catalyst deactivation. They achieved greater fatigue life by accelerating the healing kinetics [17]. Mauldin and coworkers

studied the effects of different DCPD stereoisomers on self-healing kinetics. They found that *exo*-DCPD isomer is capable of healing approximately 20 times faster than *endo*-isomer, but with a lower healing efficiency [20]. Cromwell *et al.* studied the effects of healing kinetics in an intrinsic system. They used different telechelic di-boronic ester molecules to heal 1,2-diol-containing polymer chains by crosslinking them with variable kinetics. Their research showed that the diboronic ester molecule with faster reaction kinetics can perform enhanced and accelerated healing compared to the slower one [21].

Regarding the necessity of using fast and stable healing agents to offer better performance and higher efficiency, polyurea-based extrinsic healing systems have gained attention due to their great potential. Guo *et al.* introduced the amine/isocyanate-reactive system as a promising healing agent for nonconventional environmental conditions [22]. Ma *et al.* also studied the performance of a polyurea-based self-healing system in epoxy coating via EIS tests to assess the effect of seawater immersion on the healing efficiency [23]. In one of our previous research, Koochaki *et al.,* separately encapsulated methylene diphenyl diisocyanate (MDI) and Jeffamine D230 polyetheramine, as the two portions of the polyurea-based dual capsule healing system. The performance of the bi-component system embedded in an epoxy coating was investigated by recording impedance spectra of the scratched coated steel plate immersed in 3.5 wt.% NaCl [24]. Subsequently, they studied the influence of polyetheramine modification on the healing performance of a polyurea-based dual capsule to improve the healing efficiency in wet conditions. By employing EIS as an *in situ* method, they revealed that grafting catechol side groups on the backbone of polyetheramine significantly enhanced the underwater healing performance of the resulting polyurea [25].

To deep understand the effect of healing agents' molecular characteristics on the performance of polyurea-based dual capsule healing systems, the focus of this research was devoted to *i*) the molecular weight and *ii*) functionality of amine-based agents. Therefore, three different kinds of commercially available polyetheramines were selected, while the

4

91 nature of the isocyanate counterpart was kept constant. In this regard, bi-functional Jeffamine

92 D400 (molecular weight = 400 g/mol) and tri-functional Jeffamine T403 (molecular weight

93 = 440 g/mol) are used, respectively, to study the effects of molecular weight and number of

94 active functionalities for comparison with Jeffamine D230 (230 g/mol, two functionalities)

95 taken as reference amine agent. After encapsulation of healing agents within the SAN shell,

96 the obtained MCs were embedded into an epoxy coating applied on carbon steel plates. The

97 influence of the healing agent characteristics on the kinetics and performance of the healing

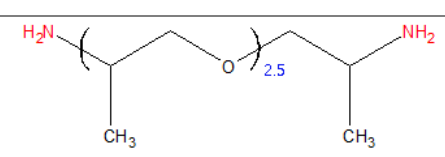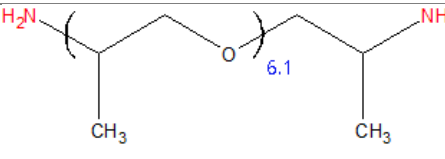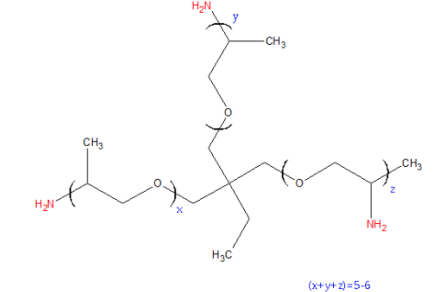98 process was evaluated by the EIS technique as well as the salt spray corrosion tests.

99 **2. Materials and Methods**

100 *2.1. Materials*

101 For the preparation of the self-healing coatings containing dual-capsule, the following

102 chemicals were purchased. Poly styrene-co-acrylonitrile (SAN, used as the capsule shell

103 material) and dimethylformamide (DMF, used as the solvent in preparing the polymer

104 solutions) were purchased from Sigma-Aldrich. Methylene diphenyl diisocyanate-based

105 prepolymer (CORONATE™1391), used as core material for assembling related MCs, was

106 provided by TOSOH Corporation. Different kinds of polyetheramines (used as core materials

107 for the second portion of MCs) were purchased from Huntsman. In particular: di-functional

108 polyetheramines with a molecular weight of 230 g/mol (Jeffamine™D230) and 400 g/mol

109 (Jeffamine™D400) were selected to study the effect of healing agent's molecular weight,

110 while a tri-functional polyetheramine (Jeffamine™T403) was chosen to study the effect of

111 healing agent's functionality, for comparison with Jeffamine™D400 having a comparable

112 mass weight. The chemical structure and viscosity of polyetheramines are summarized in

113 Table 1. An epoxy coating (epoxy resin in combination with polyaminoamide curing agent)

114 was used as the matrix to study the self-healing behaviour of the mentioned dual-capsule

5

115   system. More details about the incorporated materials can be found in our previous works

116   [24].

117   **Table 1.** The characteristics of employed polyetheramines.

Amine name	Structure	Molecular weight (g mol^{-1})	Number of – NH$_2$ functionality	Viscosity (mPa s)
Jeffamine D230 (D230)		230	2	9.5
Jeffamine D400 (D400)		400	2	22
Jeffamine T403 (T403)		440	3	72

118   *2.2. Preparation of the MCs.*

119   SAN copolymer was used as a shell for the preparation of the MCs through the

120   electrospray method. A polymer solution was prepared for each healing agent by dissolving

121   separately the shell polymer and the core material in DMF, as reported in our previous works

122   [24]. SAN concentration and core/shell weight ratio for all of the polymer solutions were

123   kept equal to 4%(w/v) and 50% (w/w), respectively. The prepared polymer solutions were

124   sprayed separately by an SP102 (Fnm co. Ltd) electrospray setup through a G23 stainless

125   steel needle. The feed rate, the applied DC potential, and the distance between the needle tip

126   and the collector (aluminium foil) were kept 0.3 ml h^{-1}, 24 kV, and 15 cm, respectively.

127   *2.3. Preparation of self-healing coatings for corrosion protection*

128   At first, amine and isocyanate-containing MCs were mixed at a 1:1 weight ratio. Then

129   the prepared Mc mixture was dispersed mechanically in the epoxy resin at a rate of 200 rpm

130   for 5 min. Subsequently, the curing agent was added to the aforementioned mixture with a

131   2:1 epoxy over curing agent weight ratio. The total MC content was kept at 3 wt% for all of

132   the applied coatings [24]. The resulted mixtures were then immediately applied on polished

133   (with 400 mesh grit paper) and degreased (with acetone) bare steel panels (Q-PANEL) by a

134   universal film applicator. The nominal thickness of the coatings was set to 100 μm.

135   All coatings, including the control sample (without MCs), were kept in the lab conditions

136   for 7 days for curing. Table 2 shows the details of the applied coatings. The cured coatings

137   were then scratched manually by a scalpel cutter (X-cut deep into the metal substrate) to

138   activate the self-healing system. Five X-cut scratches were made on each sample to evaluate

139   the healing progress via studying the corrosion resistance at different times.

140   **Table 2:** Detailed compositions of the applied coatings.

Sample name	Matrix Composition		Isocyanate MC content (wt%)	Isocyanate core material	Polyetheramine MC content (wt%)	Polyetheramine core material
	Epoxy resin	Curing agent				
c-CTRL			--	--	--	--
c-D230	EPON 828+ED180 (75:25)	Merginamid A280 (50 phr)	1.5		1.5	Jeffamine™D230
c-D400			1.5	Coronate 1391	1.5	Jeffamine™D400
c-T403			1.5		1.5	Jeffamine™T403

141   *2.4. Characterizations*

142   2.4.1. Characterization of the prepared MCs

143   FTIR (Spectrum 100 FTIR, Perkin-Elmer, USA) was conducted on the core and shell

144   materials and their corresponding prepared MCs to chemically study their structure and

145   identify any possible chemical reaction between the components. MCs were crushed prior to

146   testing and the spectra were recorded in the range 4000–400 cm^{-1}.

147 The morphology and size of the MCs were studied by SEM (JSM-5500 LV, JEOL,

148 Japan). The samples were gold-sputtered prior to SEM analysis. The size distribution

149 diagrams were prepared using Origin software by averaging the mean of 60 diameter

150 measurements. Moreover, TEM (LEO 912ab, Zeiss, Germany) was used to study the core-

151 shell structure. MCs were sprayed onto a Lacey Formvar/carbon-coated copper grid prior to

152 TEM analysis.

153 TGA tests using a TGA/DSC 2 STAR, Mettler-Toledo, Switzerland were employed to

154 confirm the successful encapsulation process and evaluation of the process yield. TGA

155 experiments were conducted from 25 °C to 500 °C (10 °C min^{-1}) under N$_2$ atmosphere.

156 2.4.2. Electrochemical assessment of the corrosion protection ability of the coatings

157 EIS tests were employed as a non-invasive monitoring technique to indirectly study the

158 self-healing process by investigating the coatings' corrosion resistance over time [26]. The

159 healing reaction was triggered by cross scratching the coatings by a #11 scalpel blade (1 × 1

160 cm length, deep into the substrate steel). To study the healing progress over time, five cross

161 scratches were made on each coating to be tested separately after keeping in the air for 2, 24,

162 48, 72, and 168 hours respectively. 168 hours (7 days) was assumed to be the maximum time

163 needed for healing in the lab conditions. All the scratched coatings were kept in the same

164 place, to ensure a uniform level of humidity that could affect the healing kinetics because of

165 the reaction with released isocyanate. Naturally aerated, near-neutral 3.5 wt% NaCl solution

166 was used as the electrolyte for testing. Moreover, to determine the healing efficiency and the

167 corrosion protection ability for each sample, the scratched coatings, which had been healed

168 in the air for 7 days, were immersed in the electrolyte solution for 14 days. The 14 days of

169 immersion were employed to provide sufficient time to reach an equilibrium condition. The

170 EIS experiments were performed by an Ivium Compactstat (Netherlands) in a 3-electrode

171 corrosion cell. An aqueous saturated calomel electrode (SCE) endowed with a Luggin

8

172   capillary, a platinum wire, and the coated steel panels (0.78 cm^2 contact area) were used as

173   the reference, counter, and working electrode, respectively. The EIS experiments were

174   conducted keeping the working electrode at the open circuit potential (OCP), sweeping the

175   frequency of the perturbing 10 mV amplitude signal in the range within 10^5 to 10^{-2} Hz.

176   2.4.3. Salt spray test

177   Salt spray test was conducted on the 7-day healed scratched coatings as a visual corrosion

178   evaluation technique to assess the healing performance, for comparison with the EIS results.

179   The experiments were done according to ASTM B117 for 72 hours by a salt spray chamber

180   (Pars Horm Co. Iran).

181   **3. Results and Discussions**

182   *3.1. Morphology of the capsules*

183   Fig. 1 shows the SEM micrographs of the mc-D400 (mc-X : MCs containing X core)

184   and mc-T403 and their corresponding size distribution diagrams. Micrographs (collected in

185   secondary electron mode) confirm that the prepared MCs have a spherical shape. The mean

186   diameters of the two types of polyetheramine-SAN MCs are measured to be 1.01±0.29 μm

187   and 0.81±0.34 μm for mc-D400 and mc-T403, respectively. The mean diameters are in good

188   agreement with the MC size of the mc-D230 (Fig. S1) [14]. The result of the distributional

189   analysis also reveals the good reproducibility of the electrospray method in terms of both

190   morphology and dimensionality of the MCs and confirms the independence of the method

191   from the employed core (see also [16], in which blends of polyetheramines were employed).

192   TEM analyses were also performed on the aforementioned MCs. According to the TEM

193   images, Fig. 2, a multicore structure was achieved for both of the core-shell MCs. A similar

194   structure was already reported for mc-D230 [14] and epoxy resin [24, 27] as core materials.

195   The SEM and TEM images of mc-Coronate 1391 and mc-D230 are also presented in the

196   supplementary file (Fig. S1 and S2), showing similar average diameters, shapes and

197   morphology. The high morphological similarity between the investigated types of MCs

198   confirms the domination rule of the shell (*i.e.,* SAN) in the encapsulation process, and

199   suggests a comparable dispersion ability of the MCs in the epoxy matrix.
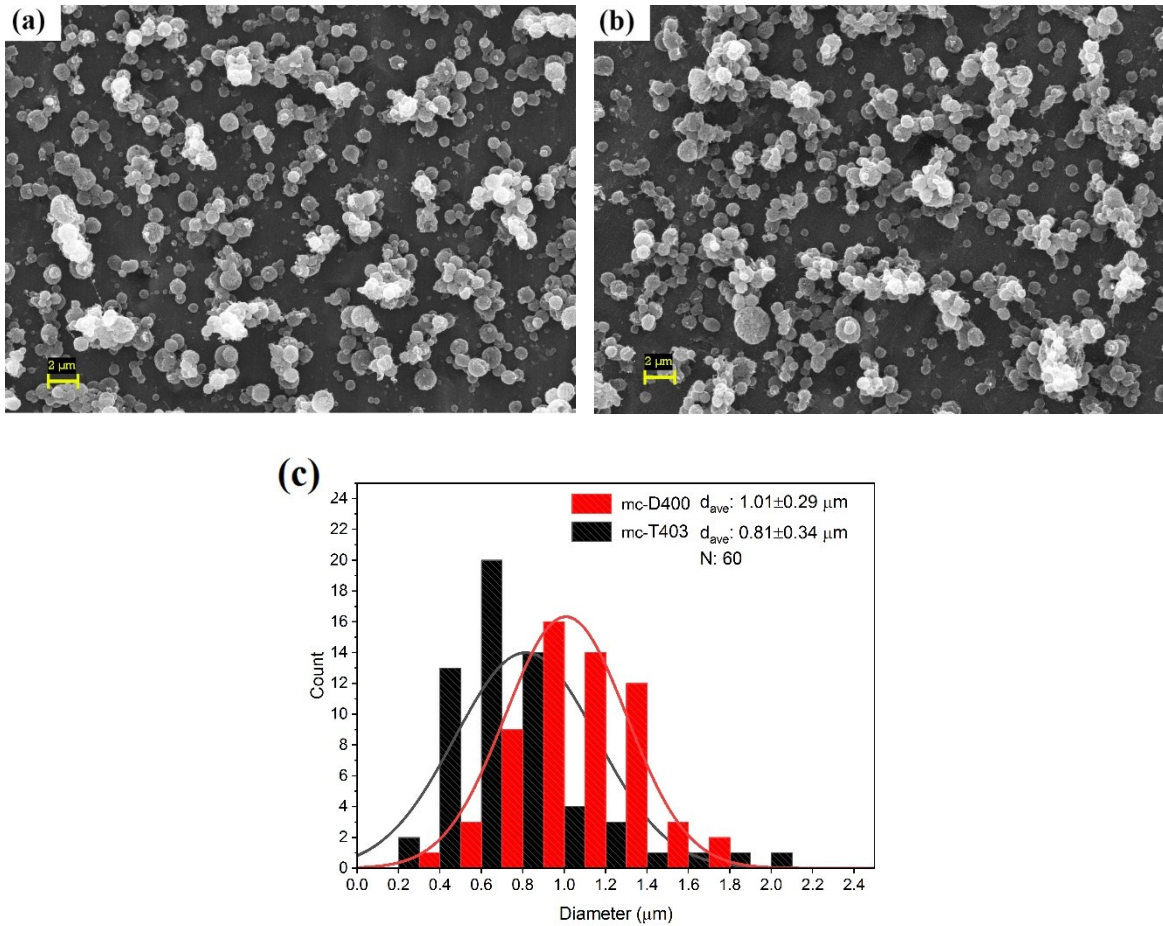
200   **Fig. 1:** SEM micrographs of the mc-D400 (a) and mc-T403 (b) and their size distribution
201   (c).

202
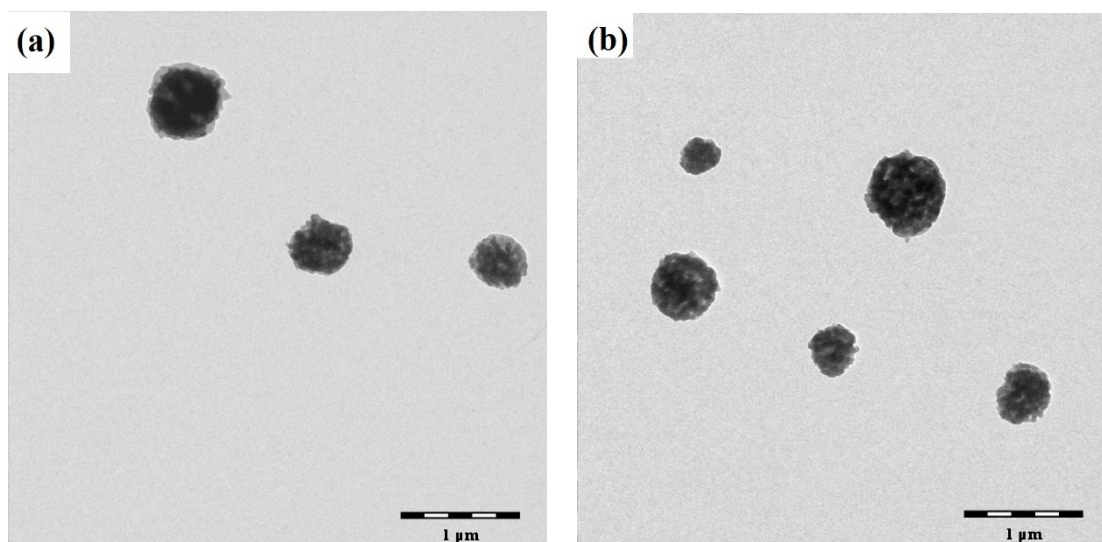
Fig. 2: TEM images of the mc-D400 (a) and mc-T403 (b).

3.2. Chemical structure of the MCs

Fig. 3 shows the FTIR spectra of the neat SAN copolymer, neat Jeffamine D400, and T403, and core-shell MCs. Regarding SAN, C–H stretching vibrations of the styrene ring are identified in the range 3085–3029 cm^{-1} while the nitrile groups are detected by the peak at 2239 cm^{-1}. Stretching and bending vibrational modes of the C–H bonds in the aliphatic segments are visible at 2924 cm^{-1} and 1452 cm^{-1}, respectively [28]. For both core materials (Jeffamine D400 and T403), the aliphatic primary amine's absorbance peaks are at 3370 cm^{-1}. The C–H stretching vibrations are observed at the peaks ranging between 2970-2950 cm^{-1} and 2885-2870 cm^{-1}, while their bending is responsible for the peak at 1455 cm^{-1}. Ether groups are characterized by a strong band at 1104-1116 cm^{-1} [29]. According to the FTIR spectra of the core-shell MCs (d,e), the characteristic peaks of shell material (*i.e.*, ca. 3030 cm^{-1}, 2240 cm^{-1}, 700 cm^{-1}) are simultaneously present with the core ones (*i.e.*, ca. 2970 cm^{-1}, 2930 cm^{-1}, 1110 cm^{-1}), just with a small shift. This is taken as proof for their co-existence in the prepared MCs with no side reactions [24]. Investigation of D230-based MCs was previously reported and discussed [14].
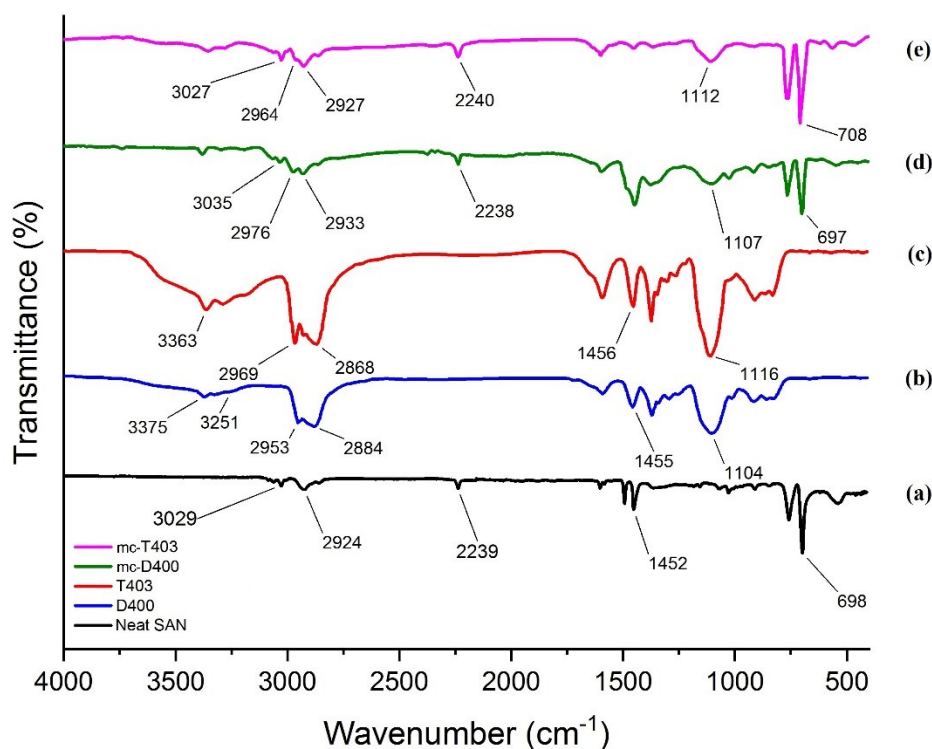
11

Fig. 3: FTIR spectra of, from bottom to top: SAN copolymer (a), D400 (b), T403 (c), and their corresponding MCs (d, e).

3.3. Thermal stability of the MCs and encapsulation yield

Fig. 4 presents the TGA results of the prepared MCs, compared with those acquired for neat core and shell components. The thermogravimetric pattern of SAN copolymer, used as shell material, showed one major decomposition stage starting at 390 °C and ending at 440 °C that results in a small amount of char which might be resulted from the acrylonitrile and styrene segments [30]. In the case of pristine core materials (*i.e.*, Jeffamine D400 and Jeffamine T403), a two-stage thermal decomposition process was observed [14]. The first stage starts at room temperature for both di- and tri-functional polyamine but it lasts at 72°C and 141°C for Jeffamine T403 and Jeffamine D400, respectively. This first small thermal stage could be attributed to the evaporation of solvents and impurities as well as lower molecular weight chains. The main decomposition stage starts at 141°C and ends at 370°C for Jeffamine D400, while for Jeffamine T403 the process occurred at a lower temperature, being triggered already at 72 °C and lasted at 290 °C.

12

236   The prepared MCs undergo three main thermal decomposition stages which occur

237   interestingly at the same temperature range as of pristine constituting materials. According

238   to the weight loss percentage of the decomposition stages and their temperature range, the

239   presence of core and shell materials together in the prepared MCs was again confirmed [28].
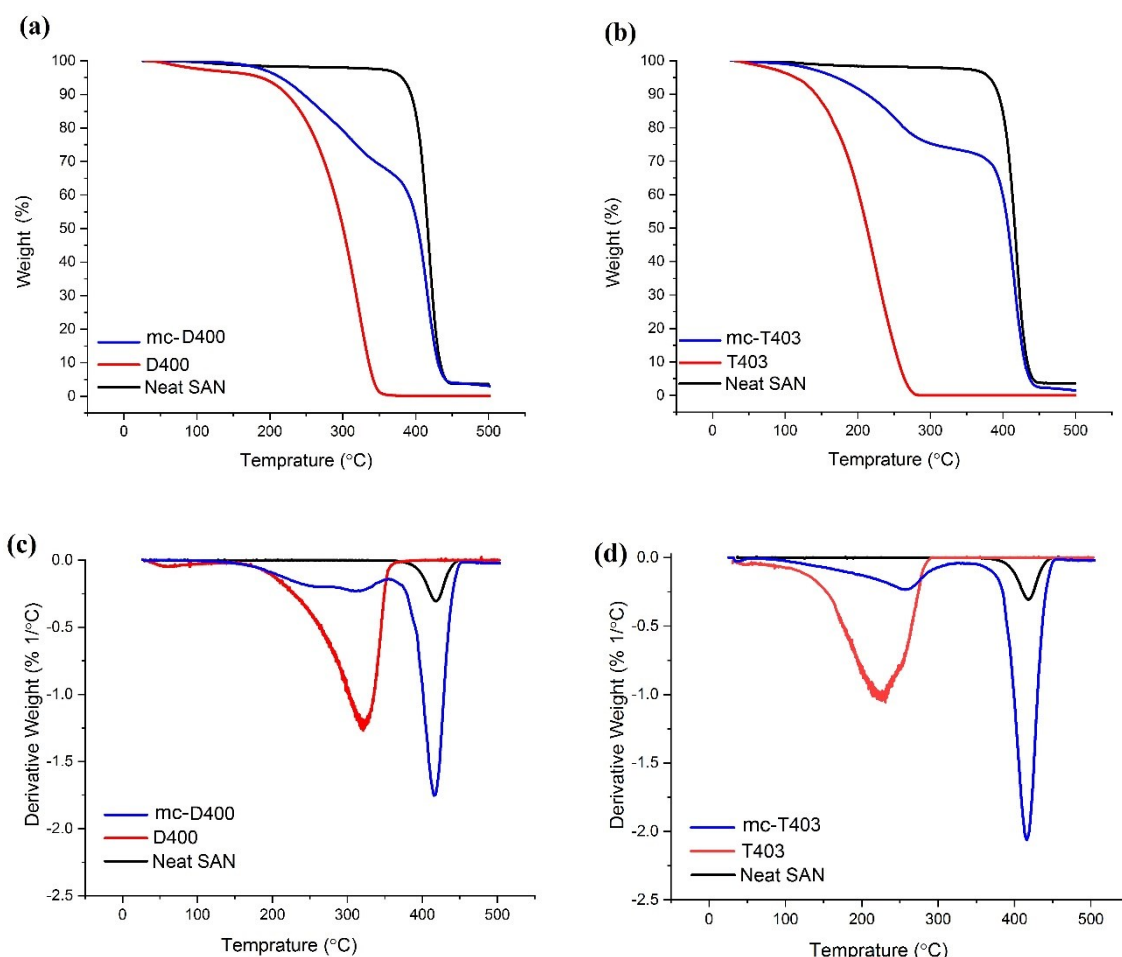
240   **Fig. 4:** Thermogravimetric analyses (top: TGA; bottom: DTGA) of the shell material
241   (SAN), core materials (D400 & T403), and their corresponding core-shell MCs.

242   Besides a further proof of the presence of two components in the prepared MCs, TGA

243   results were also used to determine i) the weight percent of the core material in the prepared

244   MCs ($\%W_{core\text{-}exp}$), and ii) the encapsulation process yield (α), according to the following

245   equation :

$$\% \, \alpha = [\%W_{core\text{-}exp} / \%W_{core\text{-}nominal}] \times 100 \tag{1}$$

13

246

247   where $W_{core-nominal}$ is the nominal weight percent of the core material, equal to the amount

248 added in the sprayed polymer solutions. The results of the quantitative analyses are

249 summarized in Table .

250

251 **Table 3:** Core material content (nominal *versus* experimental) and encapsulation yield,
252 (mc-X : MCs containing X core).

Sample	%$W_{core-nominal}$	%$W_{core-exp}$	%$α$
mc-D400	33	24	73
mc-T403	33	23	70
mc-D230[a]	33	23.5	71

253 [a] From ref. [24].

254

255   The calculated encapsulation yield for both core materials is very similar, pointing to the

256 strong robustness of the preparation protocol as it is poorly affected by characteristics of the

257 polyetheramine employed (*i.e.,* molecular weight, molecular structure, and viscosity). In

258 addition, the obtained encapsulation yields are in good agreement not only with our previous

259 report for Jeffamine D230 and Coronate 1391 MCs (71% and 68%, respectively) but also

260 with data referred to other well studied encapsulation techniques [31, 32]. One more time

261 results reported here confirmed the high reproducibility offered by the electrospray technique

262 in the preparation of polymeric core-shell capsules with average diameters around 1 μm.

263 *3.4. Assessment of the healing process through the EIS technique*

264   Fig. 5 represents the results of the time-resolved EIS experiments, carried out on the steel

265 panels coated with epoxy films (100 μm as nominal thickness). Three types of coatings were

266 investigated, sorted according to the nature of polyetheramine-bearing MCs: c-D230 (Fig.

267 5a, 5b), c-D400 (c, d), and c-T403 (e, f) samples. Kinetics and efficiency of the healing

268 reaction, as a function of polyetheramine nature, was assessed by EIS that allows providing

269 detailed information on the electrochemical behaviour of the interface(s) generated by

270 dipping the coated sample in an electrolyte solution (*i.e.,* naturally aerated 3.5 wt% NaCl).

271 The healing process was triggered by scratching the cured coatings, while the time evolution

272 of the repairing process was assessed by the variation of the electrochemical parameters

273 obtained by a quantitative interpretation of the recorded impedance spectra. To monitor the

274 evolution in time of the healing process, each scratch (deep enough to expose the underlying

275 steel surface) was left in the air, at room temperature, for an increasing period of time (up to

276 7 days, considered the time requested to assure complete healing of the scratch) before being

277 dipped into the working solution for the EIS investigation.

278   Generally, as the easiest case made of an electrochemical system that undergoes to redox

279 process (*i.e.*, an electron transfer occurring at the electrode|solution interface), the Nyquist

280 diagram (Z_{real} *vs.* $- Z_{imag}$) is characterized by a semi-circle shifted from the origin of the

281 complex plane of a quantity equal to the ohmic resistance of the system (in general the

282 solution resistance). The diameter of curves is considered as the charge transfer resistance,

283 R_{ct}. The latter is inversely proportional to the kinetic constant of the electron transfer: higher

284 R_{ct}, more sluggish the Faradaic process. If the process is kinetically limited by mass diffusion,

285 a 45°-tilted line will be depicted in the Nyquist plot (semi-infinite diffusion case), usually at

286 lower frequencies. More complex shapes can be obtained when more interfaces or more

287 processes occur in the same system, each one characterized by its own characteristic time

288 constant. Another common graphical representation of EIS results is the Bode modulus

289 diagram, in which the modulus of the impedance is directly plotted as a function of the

290 frequency of the external sinusoidal stimulus. In corrosion studies, the impedance value at

291 the lowest frequency can be taken as the total resistance of the system against corrosion [33].

292

293
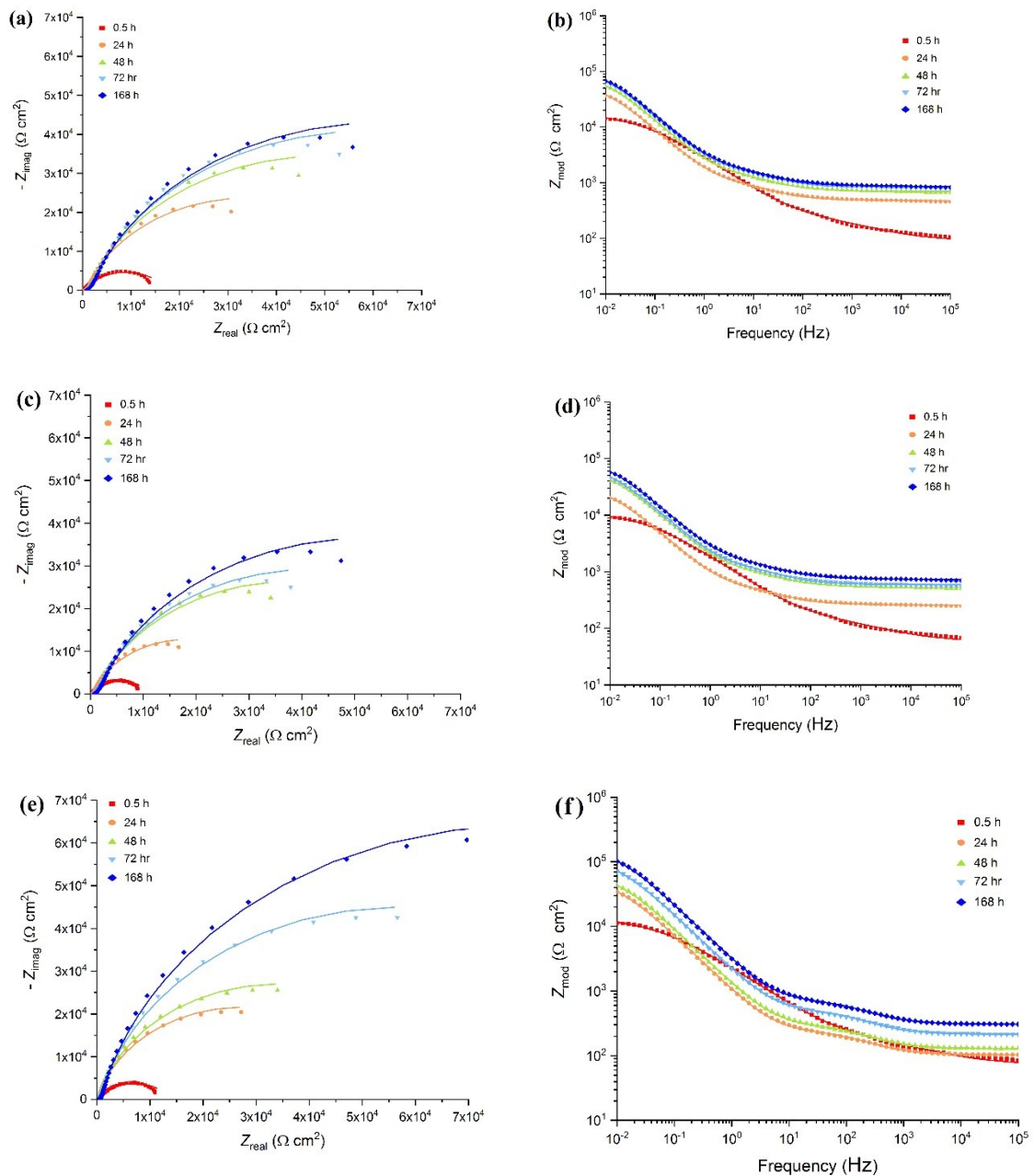
Fig. 5: Nyquist (left) and Bode plots (right) recorded at OCP of the coated samples tested at different times after being scratched and stored at open-air: c-D230 (a,b), c-D400 (c,d), and c-T403 (e,f). Electrolyte: naturally aerated, near-neutral 3.5 wt% NaCl aqueous solution. Lines are the calculated spectra by fitting the experimental data (symbols) with the equivalent circuit depicted in Fig. 6.

For the studied systems (a scratched insulating polymer film deposited on a conductive surface made of steel), a two-time constant electrical equivalent circuit (EEC) is generally used in literature to analyze the EIS results [34, 35]. In this electrical model (Fig. 6), two R-CPE parallel connections are linked in series, together with a third resistance. Each parallel

16

304   describes the behaviour of an interface: metal/solution, and polymer/solution. In more detail,

305   the resistive elements R_s, R_{ct}, and R_{coat} represent, respectively, the solution resistance, the

306   charge transfer resistance (*i.e.*, the corrosion process), and the coating resistance (the latter,

307   often called also pore resistance, is related to the porosity of the coating), while the CPE_{dl}

308   and CPE_{coat} stand for the double layer and the coating capacities, respectively.

309   In this model, the charge transfer resistance (R_{ct}) is a key parameter to investigate the

310   healing process due to its association with the Faradaic processes occurring while corrosion

311   takes place at the metal|solution interface. In fact, according to the second Ohm law, R_{ct} has

312   very interesting properties: it is inversely proportional to the exposed area of the working

313   electrode on which the corrosion occurs. As a consequence, monitoring the variation in time

314   of the numerical value of this parameter is a way to study the non-stationary barrier properties

315   of a coating subjected to the healing process. Table S1 reports the EIS parameters resulted

316   from the fitting of the experimental data with the selected EEC.
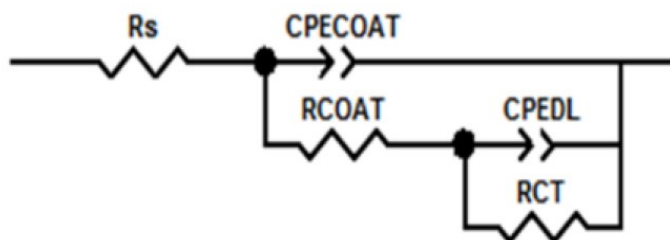
317

318   **Fig. 6:** The electric equivalent circuit used to analyze the EIS data.

319   Regarding the c-D230 sample (Fig. 5a), the results after 0.5 hr showed the lowest

320   semicircle diameter indicating the lowest corrosion resistance, but R_{ct} increased rapidly at 24

321   hours of exposition in air. This increase continued gradually, even if at a slower rate, until 72

322   hours; from that on, the charge transfer resistance remains essentially invariant up to 7 days

323   from the scratching (Fig. 7). The total impedance, estimated at the minimum frequency from

324   the Bode plots (Fig. 5b), represents the same trend in the time as well.

325   Comparing these results (absolute R_{ct} value, and its variation in time) with those

326   achieved from the c-D400 reveals the effects of a doubling of the molecular weight of the

327   healing agent. The general shape of the impedance spectra is maintained comparable with

328   that of c-D230 (Fig. 5c, 5d) as well as a comparable trend of R_{ct} variation in time (Fig. 7). It

329   suggests the effective progress of the healing process by leaving the scratched samples in the

330   air. Nonetheless, each measured impedance and R_{ct} fitted value for the c-D400 was invariably

331   lower than that detected for the analogous film embedding the lighter polyetheramine D230.

332   This can be attributed to the higher viscosity (Table 1) of D400 with respect to D230, which

333   in turns can slow down the flow of the heavier agent at the crack planes and also the lower

334   crosslink density (CLD) of the healed polymer film which allows easier water/ion

335   penetration.

336   Fig. 5e and 5f show the results of the c-T403 sample. In the case of di-amine D400, it

337   was possible to investigate the effects of a different number of functionalities of the healing

338   agent (*i.e.*, from two to three reacting sites). Contrary to the samples bearing a bi-functional

339   amine, a difference in the healing process can be seen even qualitatively by looking at the

340   Bode modulus diagrams (Fig. 5f). Starting from 24 hours after the scratching, the process

341   attributable to the establishment of a new polymer|solution interface is easily detectable in

342   the region between 10 and 100 Hz. Further confirmation of the occurrence of a more efficient

343   repairing is the monotonical increase of R_{ct} over time, characterized by a notable growth even

344   after 72 hours from the scratching (Fig. 7). In the early stage, the rate of growth of the charge

345   transfer resistance for c-T403 was lower than that acquired for c-D230 but comparable with

346   that of c-D400, despite the significantly higher viscosity of the tri-functional amine (Table

347   1). Combining these two observations (a monotonic increase of R_{ct}, that eventually reached

348   the highest value, and its slow increase during the first hours), it is plausible to state that the

349   presence of an extra $-NH_2$ functionality (resulting in a non-linear pre-polymer) guarantees to

350   the resulting polyurea an improved CLD that in turns assures a higher protection ability (*i.e.*,

351 improved barrier properties against water and ions penetration). At the same time, the

352 intrinsic 3D character of T403 healing agent counterbalances the negative effect deriving

353 from the higher viscosity that inevitably slows down its leaking and flows in the damaged

354 area.
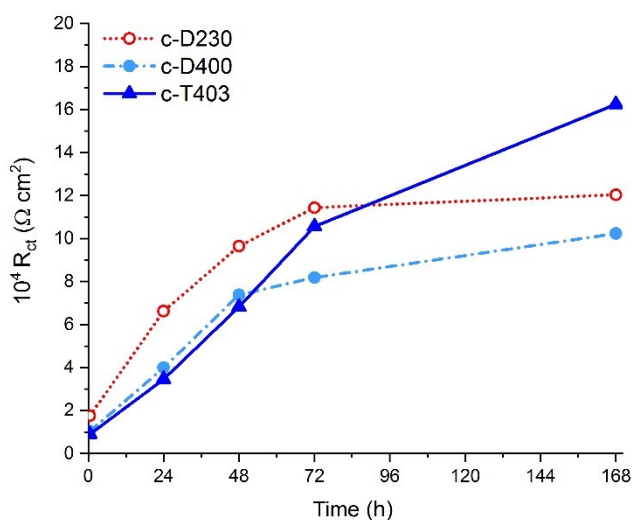
355

356 **Fig. 7:** Charge transfer resistance values (evaluated at OCP in 3.5 wt.% NaCl solution)
357 as a function of healing time (in the air) for c-D203, c-D400, and c-T403 coatings.
358

359 Therefore, Fig.7 reveals that the kinetics of the healing process is influenced by the

360 characteristics of the amine reactant as follows. The initial rapid increase of the charge

361 transfer resistance for c-D230 (in comparison with the c-D400 and c-T403 samples) can be

362 due to the fact that as the physical contact between the two functional groups (*i.e.*, $-NH_2$ and

363 $-NCO$) is mandatory for the occurrence of the stepwise polymerization reactions. In addition,

364 the lower viscosity of D230 facilitates its flow by increasing its reaction probability within

365 the damaged area in the first time frame. The slower response of c-D400 can be attributed to

366 the higher viscosity of D400, while the fact that its final R_{ct} does not change notably in

367 comparison with c-D230, is in agreement with Flory's assumptions pointing to the

368 independence between the functional groups' reactivity and the molecular weight of

369 monomers in stepwise polymerization reactions [36].

19

370   The charge transfer resistance values detected for c-T403 are the lowest in the first 48

371   hours, because, as mentioned before, the response rate on the first period after the induced

372   damage is controlled by the healing agent viscosity. On the other hand, the continuous

373   increase of R_{ct} up to 168 hours can be attributed to the higher CLD of its healing polymer

374   within the scratched area as a result of its higher functionality. Besides improved cross-

375   linking, the high viscosity of T403 can play an additional synergistic effect, if evaluated on

376   a longer time frame. In fact, while the lower viscosity of D230 brings to a fast release that

377   can block the crack path resulting in poor wetting of the entire crack plane, the higher

378   viscosity of T403 may cause a more gradual release and flow of the reacting amine with a

379   better penetration in the whole crack plane that provided an improved final healing

380   performance.

381   In order to assess the protection ability of the healed coatings over a relatively long

382   period of time, the three samples were scratched and left to heal in the air for 7 days and then

383   immersed in the electrolyte solution for 14 days. In this case, a control coating (c-CTRL) was

384   also tested for sake of comparison. Fig. 8 shows the obtained EIS spectra.

385
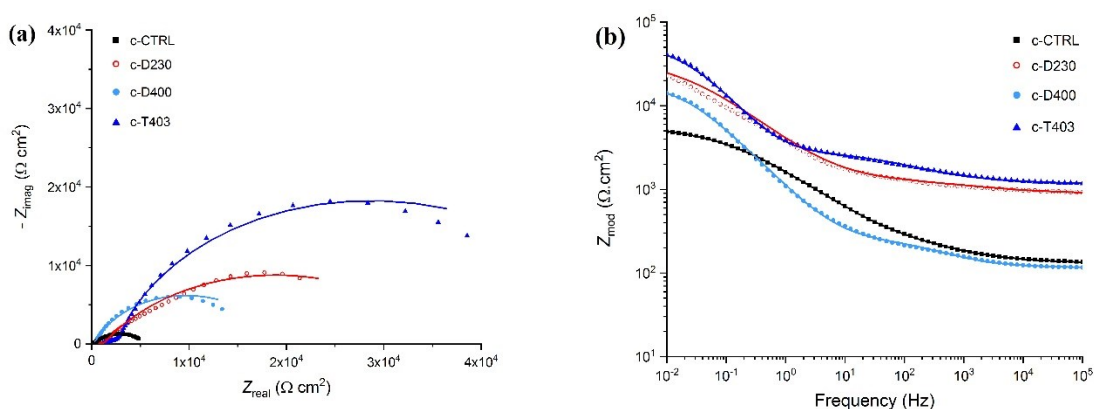
386   **Fig. 8:** EIS spectra recorded at OCP for the scratched control and healed coatings after 7
387   days of storing in air and 14 days of immersion in 3.5 wt.% NaCl solution: (a) Nyquist
388   diagrams; (b) Bode modulus plots. Lines are the calculated spectra by fitting the
389   experimental data (symbols) with the equivalent circuit depicted in Fig. 6.

390

391   The resulting spectra were fitted, using the two-time constant EEC (Fig. 6), and the

392   results are summarized in Table S2. The resulting charge transfer resistance was used to

393   estimate the healing efficiency (HE) as follows [37-39]

394    $$\%HE = \left(1 - \frac{R_{ct,0}}{R_{ct}}\right) \cdot 100 \qquad (2)$$

395   R_{ct0} and R_{ct} stand for the charge transfer resistances of the scratched control and the

396   scratched self-healing coatings, respectively, taken at the same time after scratching.

397   The calculated charge transfer resistances and their corresponding healing efficiencies

398   are summarized in Table . According to the results, the c-T403 sample showed the best

399   healing efficiency (90%), while c-D230 and c-D400 samples reached HE of 85% and 72%,

400   respectively.

401

402   **Table 4:** The calculated charge transfer resistances and the corresponding healing
403   efficiencies for the control and the self-healing coatings.

| Sample	R_{ct} (kΩ cm^2)	HE%
c-CTRL	5.35	–
c-D230	36.1	85
c-D400	18.9	72
c-T403	55.6	90

404

405   To assess the protection induced by the healed layer the EIS spectra of unscratched self-

406   healing samples were recorded after 14 days of immersion in 3.5 wt.% solutions (Fig. S3).

407   Qualitative analysis of the spectra (supported by quantitative results of the fitting, Table S3)

408   revealed an invariably worst protecting ability of the healed coatings with respect to the

409   corresponding pristine one (from 10^7 to 10^5 Ω cm^2). This loss of protection can be easily

410   attributed to a defective (*e.g.,* not perfectly compact and homogeneous) polyurea layer

411 formed between the two edges of the scratch through the reaction of the healing agents

412 released into the fracture.

413 The comparison between the impedance response of the unscratched control coating and

414 those acquired for unscratched coating containing MCs provides the evaluation of the

415 effect(s) induced in the epoxy polymer matrix by the addition of MCs. By using a one-time

416 constant EEC (*i.e.*, one couple of R and CPE elements connected in parallel), pristine control

417 coating exhibited a R_{coat} one order of magnitude higher than MC-contained coatings (10^8 and

418 10^7 Ω cm^2, respectively), at a similar C_{coat}. The lower coating resistance (attributable to a

419 slightly higher amount of defects and/or porosity of the epoxy matrix after the addition of

420 MCs) reveals a limited decrease in the barrier effect of the pristine healing coatings with

421 respect to not healing ones.

422 *3.5. Evaluation of the healing process through the salt spray test*

423 Fig. 9 shows the images of scratched coatings (control and self-healing ones) after 72

424 hours of exposure to salt spray. As can be seen, the exposed underlying steel for the control

425 sample (Fig. 9 a) is severely corroded due to the NaCl solution penetration through the scratch

426 area down to the bare metal. On the other hand, all the self-healing coatings showed a better

427 resistance against corrosion due to the reaction between released isocyanate and

428 polyetheramine healing agents that hampered the penetration of the corrosive medium by

429 sealing (at least partially) the scratch area as a result of the polyurea formation. According to

430 the images, the c-T403 sample (Fig. 9 d) showed the minimum amount of rust indicating the

431 most effective corrosion protection after damaging of the series, followed by c-D230 (Fig. 9

432 b) and c-D400 (Fig. 9 c). The salt spray test reveals the efficient performance of the

433 incorporated self-healing polyetheramine agents, representing a practical and "easy-to-

434 assess" corrosion test that confirms the results argued from the EIS investigation.
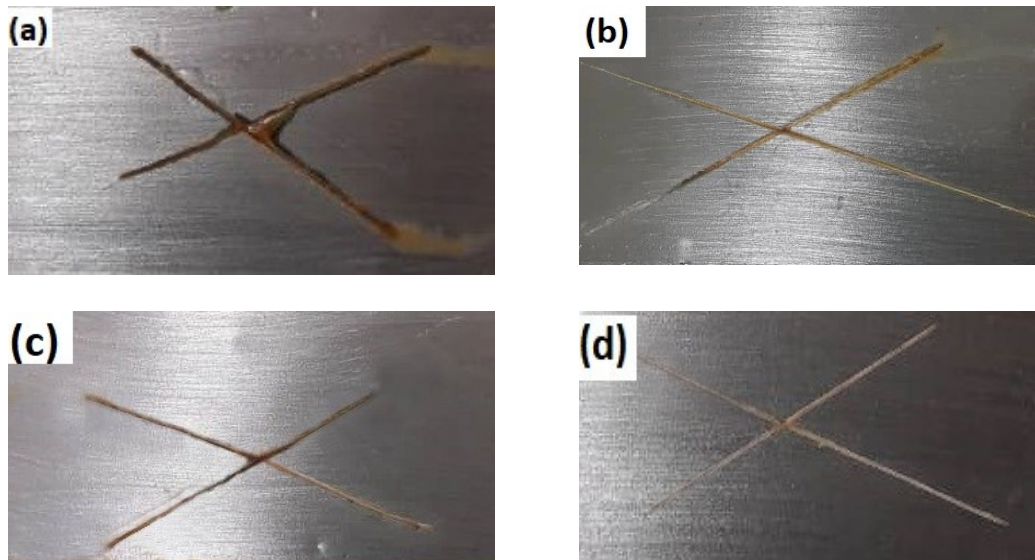
Fig. 9: Salt spray results after 72 hr for: (a) c-CTRL, (b) c-D230, (c) c-D400, and (d) c-T403.

4. Conclusions

As part of a broader systematic study carried out by the group, the effects of molecular characteristics of polyetheramines on i) the kinetics of the healing process and ii) the related self-healing performance were studied to obtain more efficient corrosion protection coatings that limit the detrimental effects of damages affecting the physical integrity of the polymeric barrier. A dual capsule extrinsic system was embedded into an epoxy matrix to prepare self-healing coatings that exploit the stepwise polymerization reaction between isocyanate and amine functional groups for the formation of a repairing polyurea film. While the isocyanate component was kept constant in the formulations, three types of polyetheramines varying in molecular weight and functionality were used, separately, as the second reacting agent. Each element of the reacting couple was firstly encapsulated by electrospray into spherical core-shell MCs (diameter < 2 μm) and then embedded into the epoxy matrix. EIS technique was employed as a non-destructive investigation method to indirectly monitor the time evolution of the healing reaction (carried out in the air in the same laboratory, to omit effects of air humidity on isocyanate) by recording impedance spectra in 3.5 wt.% NaCl solution. The

452 investigation revealed that a lower molecular weight amine provides a faster response of the

453 healing system due to the easier flow into the crack caused, in turn, by the lower viscosity.

454 On the other hand, an increase of the molecular weight (D400) corresponds to slower kinetics

455 during the early stages of the healing process, due to the increased viscosity of the reactant,

456 but without significantly compromising the overall performance. In addition, by increasing

457 the functionality (T403) a monotonically increase of the corrosion protection ability of the

458 healed coating was obtained, without unduly affecting the speed of the repairing process. The

459 significantly different trend over time of the corrosion protection recovery for T403 amine

460 has been attributed to the higher crosslinking density and the resulting better-protecting

461 properties of the healed area, potentially assisted by the slower diffusion of the healing agent

462 driving to a more compact polyurea matrix. As a result, the healing efficiency, estimated

463 from the EIS results, moves from ca. 72% for the heavier, di-functional D400 to ca. 90% for

464 the coating embedding the trifunctional T403 polyetheramine. The salt spray testing

465 confirmed, through a visual investigation, the aforementioned trend in the corrosion

466 protection performance for the prepared self-healing coatings.

467 **Author Contributions:**

468 **Mohammad Sadegh Koochaki**: Conceptualization, Methodology, Investigation, Data

469 Curation, Writing - Original Draft, Writing - Review & Editing, Visualization **Rasoul**

470 **Esmaeely Neisiany**: Conceptualization, Methodology, Validation, Data Curation, Writing -

471 Original Draft, Writing - Review & Editing, Visualization **Saied Nouri Khorasania**:

472 Conceptualization, Validation, Resources, Writing - Original Draft, Writing - Review &

473 Editing, Supervision, Project administration, Funding acquisition **Ali Ashrafi**: Data

474 Curation, Writing - Original Draft, Writing - Review & Editing, Supervision **Stefano P.**

475 **Trasatti**, Methodology, Validation, Resources, Writing - Review & Editing, Supervision

476 **Mirko Magni**: Methodology, Data Curation, Writing - Original Draft, Writing - Review &

477 Editing, Supervision

478

487

488 **Declaration of interests:**

489 The authors declare that they have no known competing financial interests or personal

490 relationships that could have appeared to influence the work reported in this paper.

491

492 **References**

493 [1] A. Davoodi, S. Honarbakhsh, G.A. Farzi, Evaluation of corrosion resistance of
494 polypyrrole/functionalized multi-walled carbon nanotubes composite coatings on 60Cu–
495 40Zn brass alloy, Progress in Organic Coatings, 88 (2015) 106-115.
496 [2] T. Liu, J. Wei, L. Ma, S. Liu, D. Zhang, H. Zhao, Effect of polyaniline-based plate on the
497 anticorrosion performance of epoxy coating, Progress in Organic Coatings, 151 (2021)
498 106109.
499 [3] D.Y. Wu, S. Meure, D. Solomon, Self-healing polymeric materials: A review of recent
500 developments, Progress in Polymer Science, 33 (2008) 479-522.
501 [4] R. Malekkhouyan, R.E. Neisiany, S.N. Khorasani, O. Das, F. Berto, S. Ramakrishna, The
502 influence of size and healing content on the performance of extrinsic self-healing coatings,
503 Journal of Applied Polymer Science, 138 (2021) 49964.

504 [5] P. Panahi, S.N. Khorasani, M.S. Koochaki, M. Dinari, O. Das, R.E. Neisiany, Synthesis
505 of Cloisite 30B-acrylamide/acrylic acid nanogel composite for self-healing purposes,
506 Applied Clay Science, 210 (2021) 106174.

507 [6] W. Hao, Y. Liu, H. Zhou, H. Chen, D. Fang, Preparation and characterization of 3D
508 printed continuous carbon fiber reinforced thermosetting composites, Polymer Testing, 65
509 (2018) 29-34.

510 [7] Z. Wang, X. Lu, S. Sun, C. Yu, H. Xia, Preparation, characterization and properties of
511 intrinsic self-healing elastomers, Journal of Materials Chemistry B, 7 (2019) 4876-4926.

512 [8] S. Wang, M.W. Urban, Self-healing polymers, Nature Reviews Materials, 5 (2020) 562-
513 583.

514 [9] Ö. Tezel, A. Beyler Çiğil, M.V. Kahraman, Dual microcapsules based
515 epoxy/polyethyleneimine autonomous self-healing system for photo-curable coating,
516 Polymers for Advanced Technologies, 32 (2021) 553-563.

517 [10] E.N. Brown, S.R. White, N.R. Sottos, Retardation and repair of fatigue cracks in a
518 microcapsule toughened epoxy composite–Part I: Manual infiltration, Compos Sci Technol,
519 65 (2005) 2466-2473.

520 [11] S. Lang, Q. Zhou, Synthesis and characterization of poly(urea-formaldehyde)
521 microcapsules containing linseed oil for self-healing coating development, Progress in
522 Organic Coatings, 105 (2017) 99-110.

523 [12] Ö. Tezel, A.B. Çiğil, M.V. Kahraman, Design and development of self-healing coating
524 based on thiol–epoxy reactions, Reactive and Functional Polymers, 142 (2019) 69-76.

525 [13] M.W. Keller, S.R. White, N.R. Sottos, A self- healing poly (dimethyl siloxane)
526 elastomer, Adv Funct Mater, 17 (2007) 2399-2404.

527 [14] S.H. Cho, S.R. White, P.V. Braun, Self- healing polymer coatings, Adv Mater, 21
528 (2009) 645-649.

529 [15] R. Esmaeely Neisiany, M.S. Enayati, P. Sajkiewicz, Z. Pahlevanneshan, S.
530 Ramakrishna, Insight Into the Current Directions in Functionalized Nanocomposite
531 Hydrogels, Frontiers in Materials, 7 (2020) 25.

532 [16] Z. Wang, L. Scheres, H. Xia, H. Zuilhof, Developments and Challenges in Self-Healing
533 Antifouling Materials, Advanced Functional Materials, n/a (2020) 1908098.

534 [17] A. Jones, J. Rule, J. Moore, N. Sottos, S. White, Life extension of self-healing polymers
535 with rapidly growing fatigue cracks, J R Soc Interface, 4 (2007) 395-403.

536 [18] X.K.D. Hillewaere, F.E. Du Prez, Fifteen chemistries for autonomous external self-
537 healing polymers and composites, Progress in Polymer Science, 49-50 (2015) 121-153.

538 [19] A.S. Jones, J.D. Rule, J.S. Moore, S.R. White, N.R. Sottos, Catalyst morphology and
539 dissolution kinetics of self-healing polymers, Chem Mater, 18 (2006) 1312-1317.

540 [20] T.C. Mauldin, J.D. Rule, N.R. Sottos, S.R. White, J.S. Moore, Self-healing kinetics and
541 the stereoisomers of dicyclopentadiene, J R Soc Interface, 4 (2007) 389-393.

542 [21] O.R. Cromwell, J. Chung, Z. Guan, Malleable and self-healing covalent polymer
543 networks through tunable dynamic boronic ester bonds, J Am Chem Soc, 137 (2015) 6492-
544 6495.

545 [22] M. Guo, W. Li, N. Han, J. Wang, J. Su, J. Li, X. Zhang, Novel dual-component
546 microencapsulated hydrophobic amine and microencapsulated isocyanate used for self-
547 healing anti-corrosion coating, Polymers, 10 (2018) 319.
548 [23] Y. Ma, Y. Zhang, J. Liu, Y. Sun, Y. Ge, X. Yan, J. Wu, Preparation and Characterization
549 of Ethylenediamine-Polyurea Microcapsule Epoxy Self-Healing Coating, Materials, 13
550 (2020) 326.
551 [24] M.S. Koochaki, S.N. Khorasani, R.E. Neisiany, A. Ashrafi, M. Magni, S.P. Trasatti,
552 Facile strategy toward the development of a self-healing coating by electrospray method,
553 Mater Res Express, 6 (2019) 116444.
554 [25] M.S. Koochaki, S.N. Khorasani, R.E. Neisiany, A. Ashrafi, S.P. Trasatti, M. Magni, A
555 highly responsive healing agent for the autonomous repair of anti-corrosion coatings on wet
556 surfaces. In operando assessment of the self-healing process, Journal of Materials Science,
557 56 (2021) 1794-1813.
558 [26] C. Zhang, H. Wang, Q. Zhou, Preparation and characterization of microcapsules based
559 self-healing coatings containing epoxy ester as healing agent, Progress in Organic Coatings,
560 125 (2018) 403-410.
561 [27] I.L. Hia, P. Pasbakhsh, E.-S. Chan, S.-P. Chai, Electrosprayed multi-core alginate
562 microcapsules as novel self-healing containers, Sci Rep, 6 (2016) 34674.
563 [28] R.E. Neisiany, J.K.Y. Lee, S.N. Khorasani, S. Ramakrishna, Towards the development
564 of self-healing carbon/epoxy composites with improved potential provided by efficient
565 encapsulation of healing agents in core-shell nanofibers, Polym Test, 62 (2017) 79-87.
566 [29] B. Chen, J. Li, T. Liu, Z. Dai, H. Zhao, Facile preparation of epoxy based elastomers
567 with tunable T gs and mechanical properties, RSC Adv, 8 (2018) 13474-13481.
568 [30] T.J. Xue, C.A. Wilkie, Thermal degradation of poly (styrene-g-acrylonitrile), Polym
569 Degrad Stab, 56 (1997) 109-113.
570 [31] M. Huang, J. Yang, Facile microencapsulation of HDI for self-healing anticorrosion
571 coatings, J Mater Chem, 21 (2011) 11123-11130.
572 [32] D.A. McIlroy, B.J. Blaiszik, M.M. Caruso, S.R. White, J.S. Moore, N.R. Sottos,
573 Microencapsulation of a reactive liquid-phase amine for self-healing epoxy composites,
574 Macromolecules, 43 (2010) 1855-1859.
575 [33] E. Bakhshandeh, A. Jannesari, Z. Ranjbar, S. Sobhani, M.R. Saeb, Anti-corrosion hybrid
576 coatings based on epoxy–silica nano-composites: Toward relationship between the
577 morphology and EIS data, Progress in Organic Coatings, 77 (2014) 1169-1183.
578 [34] W. Wang, L. Xu, X. Li, Z. Lin, Y. Yang, E. An, Self-healing mechanisms of water
579 triggered smart coating in seawater, J Mater Chem A, 2 (2014) 1914-1921.
580 [35] M. Hasanzadeh, M. Shahidi, M. Kazemipour, Application of EIS and EN techniques to
581 investigate the self-healing ability of coatings based on microcapsules filled with linseed oil
582 and CeO2 nanoparticles, Prog Org Coat, 80 (2015) 106-119.
583 [36] P.J. Flory, Principles of polymer chemistry, Cornell University Press, 1953.
584 [37] A.M. Atta, O.E. El-Azabawy, H. Ismail, M. Hegazy, Novel dispersed magnetite core–
585 shell nanogel polymers as corrosion inhibitors for carbon steel in acidic medium, Corros Sci,
586 53 (2011) 1680-1689.

587   [38] A. Atta, G. El-Mahdy, H. Al-Lohedan, S. Al-Hussain, Synthesis of environmentally
588   friendly highly dispersed magnetite nanoparticles based on rosin cationic surfactants as thin
589   film coatings of steel, Int J Mol Sci, 15 (2014) 6974-6989.
590   [39] E. Rezvani Ghomi, R. Esmaeely Neisiany, S. Nouri Khorasani, M. Dinari, S. Ataei, M.S.
591   Koochaki, S. Ramakrishna, Development of an epoxy self-healing coating through the
592   incorporation of acrylic acid-co-acrylamide copolymeric gel, Progress in Organic Coatings,
593   149 (2020) 105948.
594